ELSEVIER

Journal of Biomechanics 39 (2006) 1191–1200

JOURNAL OF BIOMECHANICS

www.elsevier.com/locate/jbiomech
www.JBiomech.com

# In vivo micro particle image velocimetry measurements of blood-plasma in the embryonic avian heart

Peter Vennemann[a,*], Kenneth T. Kiger[b], Ralph Lindken[a], Bianca C.W. Groenendijk[c], Sandra Stekelenburg-de Vos[d], Timo L.M. ten Hagen[e], Nicolette T.C. Ursem[d], Rob E. Poelmann[c], Jerry Westerweel[a], Beerend P. Hierck[c]

[a]*Laboratory for Aero- and Hydrodynamics, Delft University of Technology, Leeghwaterstraat 21, 2628 CA Delft, The Netherlands*
[b]*Department of Mechanical Engineering, University of Maryland, USA*
[c]*Department of Anatomy and Embryology, Leiden University MC, The Netherlands*
[d]*Department of Obstetrics and Gynaecology, Erasmus MC Rotterdam, The Netherlands*
[e]*Department of Surgical Oncology, Erasmus MC Rotterdam, The Netherlands*

Accepted 15 March 2005

**Abstract**

The measurement of blood-plasma velocity distributions with spatial and temporal resolution in vivo is inevitable for the determination of shear stress distributions in complex geometries at unsteady flow conditions like in the beating heart. A non-intrusive, whole-field velocity measurement technique is required that is capable of measuring instantaneous flow fields at sub-millimeter scales in highly unsteady flows. Micro particle image velocimetry (μPIV) meets these demands, but requires special consideration and methodologies in order to be utilized for in vivo studies in medical and biological research.

We adapt μPIV to measure the blood-plasma velocity in the beating heart of a chicken embryo. In the current work, bio-inert, fluorescent liposomes with a nominal diameter of 400 nm are added to the flow as a tracer. Because of their small dimension and neutral buoyancy the liposomes closely follow the movement of the blood-plasma and allow the determination of the velocity gradient close to the wall. The measurements quantitatively resolve the velocity distribution in the developing ventricle and atrium of the embryo at nine different stages within the cardiac cycle. Up to 400 velocity vectors per measurement give detailed insight into the fluid dynamics of the primitive beating heart. A rapid peristaltic contraction accelerates the flow to peak velocities of 26 mm/s, with the velocity distribution showing a distinct asymmetrical profile in the highly curved section of the outflow tract.

In relation to earlier published gene-expression experiments, the results underline the significance of fluid forces for embryonic cardiogenesis. In general, the measurements demonstrate that μPIV has the potential to develop into a general tool for instationary flow conditions in complex flow geometries encountered in cardiovascular research.


*Keywords:* Blood flow; Cardiac development; Flow shear stress; Gene expression; Imaging

## 1. Introduction

The need to measure both spatially and temporally resolved fluid velocity fields exists in numerous areas of medical and biological research. For example, two-dimensional blood velocity measurements are suitable for quantitatively monitoring the microcirculation within well-defined regions of the vasculature. Furthermore, the measurement of spatial velocity fields is a minimum requirement for determining hydrodynamic wall shear stresses on the surface of moving boundaries such as those found in the heart. The wall shear stress is an important parameter in fundamental areas of angiogenesis and cardiology and plays a key role in problems

*Corresponding author. Tel.: +31 15 278 4194; fax: +31 15 278 2947.
*E-mail address:* p.vennemann@wbmt.tudelft.nl (P. Vennemann).

0021-9290/$ - see front matter © 2005 Elsevier Ltd. All rights reserved.
doi:10.1016/j.jbiomech.2005.03.015

such as the pathology of atherosclerosis (Malek et al., 1999; Liepsch, 1990) and the study of cardiogenesis (Hove et al., 2003; Hogers et al., 1999). Experimental values for the wall shear stress, $\tau$, can be extracted from a velocity field by the calculation of the wall-normal velocity gradients, $\mathrm{d}u/\mathrm{d}n$:

$$\tau = \eta \frac{\mathrm{d}u}{\mathrm{d}n}, \tag{1}$$

where $\eta$ is the dynamic viscosity of the fluid and is either presumed to be known from literature or can be estimated based on the local flow parameters (i.e., hematocrit value and shear rate).

The development of the method presented in this paper is motivated by the need for a general measurement technique that is applicable to the aforementioned fields of interest. The investigation of the influence of hemodynamically induced wall shear stress on cardiogenesis serves as a particular test case. Placental blood flow is thought to play a significant role in normal and abnormal human heart development (Hogers et al., 1999). For studying this relationship experimentally, an embryonic chicken is used as an animal model. Fig. 1 displays a chicken embryo after approximately 50 h of incubation, which corresponds to development Stage 15 (Hamburger and Hamilton, 1951). On the right and left side of the image one can clearly see extraembryonic vitteline vessels that serve the same function as the placenta in a mammalian embryo. It has been shown that obstructing venous flow by closing one of these vessels with a clip results in re-routing of the venous return to the heart, the alteration of blood flow profiles through the heart, and the development of specific cardiovascular malformations (Hogers et al., 1999).

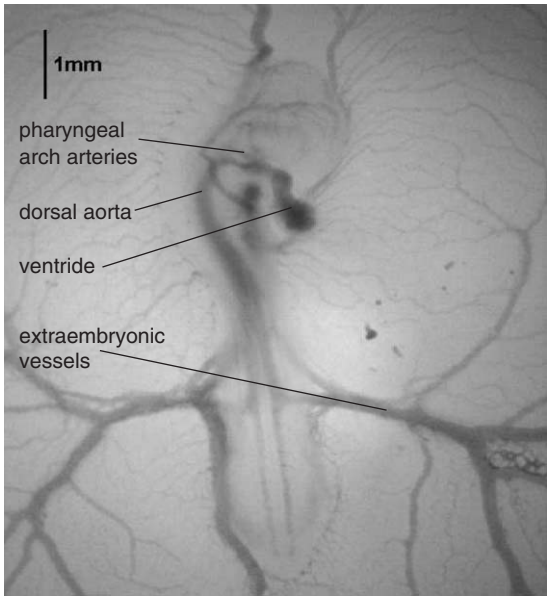


Fig. 1. Stage 15 embryo after approximately 50 h of incubation.

From in vitro flow studies on the vascular endothelium, it is known that flow induced shear stress modulates gene expression (Topper and Gimbrone Jr., 1999). The present in vivo measurement system has been developed with the long-term goal of combining velocity field measurements with the visualization of gene expression to find a relationship between extraembryonic flow and cardiogenesis. In this paper we describe the measurement technique and the application to the flow in the heart.

Particle image velocimetry (PIV) provides instantaneous velocity fields at a spatial resolution in the order of hundred nanometers under ideal conditions (Tretheway and Meinhart, 2002; Westerweel et al., 2004). The technique is briefly described in the Materials and methods section; detailed descriptions can be found in the works by Westerweel (1993) and Raffel et al. (1998). Advantageous for determining wall shear stress is the fact that our implementation of PIV also allow for a precise determination of the flow boundary. This holds in particular for situations where the boundary is not stationary, like in the case of a beating heart. Such measurements would be impracticable with single point-measurement techniques like laser-Doppler-velocimetry (LDV). MRI is difficult to apply on highly instationary flows, because of its limited temporal resolution (Liepsch, 2002).

In many applications, PIV has developed into the method of choice wherever spatial velocity information is required (Adrian, 1991). More recently Santiago et al. (1998) introduced a modified system which enabled PIV using a microscope, which is commonly referred to as μPIV. Several authors have demonstrated the applicability of μPIV or related techniques to study blood flow. Tangelder et al. (1986) labelled blood platelets with a fluorescent dye to measure steady flow velocities in arterioles of the rabbit mesentery by determining the velocity of individual particles. Individual velocity measurements at different radial positions of the blood vessel were assembled to estimate the velocity profile. Smith et al. (2003) refined this method by injecting fluorescent microspheres (500 nm diameter) into the mouse cremaster muscle venules, although only the velocities of up to four particles at irregular distances above the glycocalyx layer were used to estimate the velocity profile. This method is only useful in the special case of steady flow conditions.

Hitt et al. (1996) applied a correlation technique to video images of the venous flow in the hamster cremaster muscle. Tsukada et al. (2000) and Sugii et al. (2002a,b) used μPIV to measure red blood cell velocity profiles in mesentery vessels of rats. Hove et al. (2003) followed the course of small groups of erythrocytes through the heart of a zebrafish embryo. In all of these studies, erythrocytes were used as tracer particles.

As will be explained in the Discussion section of this paper, tracer particles that are significantly smaller than the large erythrocytes (which have a diameter of eight to ten micrometers) enhance resolution and reliability of the measurement. Accordingly the present work focuses on the enhancement of the accuracy of in vivo μPIV measurements by using fluorescent, long-circulating liposomes that have a nominal diameter of 400 nm as tracer particles. The liposome tracer particles are illuminated by a pulsed laser that is used in conjunction with an acoustic pulsed Doppler velocimeter probe (Ursem et al., 2001) to provide time-resolved ensemble average measurements throughout the cardiac cycle.

## 2. Materials and methods

### 2.1. Measurement principle

The basic principle behind PIV uses two sequential digital images that are taken from a flow which is visualized by adding small tracer particles. The displacement of the particles in the second image, relative to the position of the particles in the first image, is a measure of the motion of the fluid. The displacement of the particles is obtained by means of a two-dimensional cross-correlation using a computer. This means that a small interrogation window of the first image is correlated with varying sections of the second image, such that the correlation magnitude between the image areas is maximized. The position of maximum correspondence is the most probable displacement of the particle pattern in the interrogation window. The local velocity is calculated by dividing the displacement of the particle pattern by the given time difference between the two images (Adrian, 1991; Raffel et al., 1998). For typical macroscale PIV applications, a two-dimensional measurement plane is formed by illuminating only a thin plane of the flow with a well-defined laser light sheet, whereas for microscale applications the strongly limited depth-of-focus of the microscope objective is used to sample a thin plane in which the particles are sharply imaged (Santiago et al., 1998; Meinhart et al., 1999; Olsen and Adrian, 2000).

### 2.2. Animals

Fertilized White Leghorn eggs were incubated until they reach development Stage 15 (according to the staging criteria of Hamburger and Hamilton (1951)). Part of the egg shell is removed to establish optical access to the embryo. To prevent desiccation by evaporation, the whole *area vasculosa* is covered with a film of purified mineral oil (*paraffinum subliquidum*). To maintain a constant temperature of 37 °C the egg is partially immersed in a constant temperature water bath during the experiment. A stable heart rate of about $120 \pm 4$ beats per minute indicated unperturbed conditions throughout the analysis. The cardiac outflow tract (developing right ventricle) containing the endocardial cushions is visualized without mechanical manipulation of the embryo (see Fig. 1). High levels of mRNA from genes that have been shown to upregulate expression under high shear stress conditions can be detected in this section (Groenendijk et al., 2004). The developing atrial compartment could be measured from an embryo that showed a natural "right-side-down" positioning on the yolk sac.

### 2.3. Experimental set-up

Fig. 2 gives an overview of the experimental set-up. It mainly consists of a fluorescence microscope with a dual-cavity Nd:YAG laser lightsource, fitted with a double-frame camera. Laser and camera are synchronized by a timing unit built into a PC. The data is stored on the same PC. Fig. 2 further shows an ultrasound Doppler velocimeter and an additional PC to trigger the timing unit with the heartbeat of the embryo. The components of the set-up and their function is described in detail in the following paragraphs.

The blood flow is observed through a 10× magnification apochromatic objective with an numerical aperture, NA = 0.4 (*Leica HC PLAN APO* 10 × /0.40). The microscope (*Leica DM4000B*) is equipped with a filter system suitable for 532 nm excitation and 560 nm peak emission wavelength.

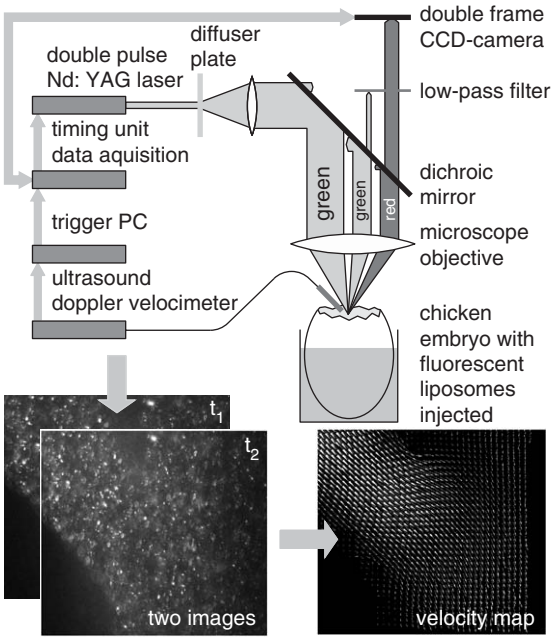


Fig. 2. μPIV set-up, using a fluorescence microscope. A dichroic mirror and a low-pass filter allow only the light emitted by the fluorescent tracer particles to reach the camera.

The dual-cavity, pulsed Nd:YAG laser (*New Wave MiniLase II PIV*) with a frequency doubled output wavelength of $\lambda = 532\,\text{nm}$ and a pulse duration of approximately 6 ns is attached at the impinging-light port of the microscope. The dual-cavity laser enables one to adjust the time delay between two pulses to any value, limited by a minimal camera interframing time of 200 ns. In this way the time difference between the laser pulses can be easily adapted to the expected velocities. The laser is operated at approximately 0.5 mJ light energy per pulse. To attenuate speckle noise due to the coherent character of laser light, a $10^{\circ}$*LSD® light shaping diffuser* is mounted into the light path. The light is collimated to a ray bundle 30 mm in diameter before it enters the microscope.

At the documentation tube of the microscope, a 12-bit double-frame charge coupled device (CCD) camera with enhanced quantum efficiency and a resolution of 1376 × 1040 pixels is fitted (*LaVision Imager Intense*, identical to *Sensicam QE* by *PCO*). The double-frame feature of this camera allows for the acquisition of two images prior to read-out, by buffering the first image in a non-light sensitive area of the CCD chip. In this way, two images can be taken with a minimum interframing time of 200 ns, although the framing rate of the camera is only 4.5 Hz in this operation mode. Short interframing times enable the measurement of high velocities at high magnification.

The synchronization of the camera, the laser, data acquisition and data storage are done by means of a commercially available computer system with a built in timing unit (*LaVision PTU 8*).

For the synchronization of the data-acquisition PC to the cardiac cycle of the chicken embryo, the acoustic probe of a 20-MHz ultrasound pulsed Doppler velocimeter (*model 545C-4, Iowa Doppler Products*) is placed close to the dorsal aorta of the embryo. Moving blood cells reflect a frequency shifted echo which is transmitted to a computer after being quadrature demodulated, low-pass filtered and digitized. A *LabVIEW* (*National Instruments*) program extracts the maximum directional velocity from the audio signals in real-time by means of fast Fourier transformation (FFT) following the bispectral analysis methods demonstrated by Ursem et al. (2001). The camera and laser are then triggered based on a threshold and slope criterion of the maximum velocity in conjunction with a constant, adjustable delay.

### 2.4. Tracer particles

The tracer particles are injected into one of the vitelline veins using an approximately 10 μm thick glass-needle. Fig. 3 illustrates the principle structure of the fluorescent liposome tracer particles used in this study. The liposome membrane consists of phospholipids that form a spherically closed bilayer to shield their hydrophobic tails against the surrounding aqueous solution. Rhodamine tagged phospholipids are used for visualization of the liposomes. So called long-circulating "stealth" liposomes are created by additionally coating their surface with long chains of polyethylene glycol (PEG) to prevent various proteins and immune-system molecules from adhering to the liposome surface (Woodle and Lasic, 1992). In the early chicken embryo, where no immune system is yet present, the PEG-coating prevents the particles from adhering to the walls of the vasculature. These liposomes are biodegradable and can therefore be used in non-final animal experiments (Woodle and Lasic, 1992).

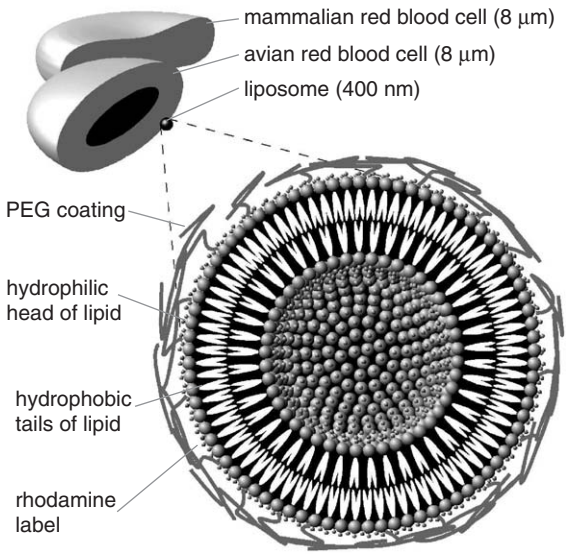


Fig. 3. Schematic section of a PEG-coated liposome. The hydrophilic heads of the lipids are labeled with rhodamine molecules. The PEG-coating prevents the particles from adhering to the vessel walls.

### 2.5. Evaluation

Meinhart et al. (2000) have shown that the reliability of a μPIV-evaluation can be significantly enhanced by summing up the PIV correlation results of multiple measurements (ensemble correlation). This technique is especially advantageous at conditions with low seeding density and poor particle visibility over the background glow, which are typically found in blood flow applications. The ensemble correlation technique requires a set of measurements at exactly the same flow conditions. This is the reason why proper phase-locking of the data-acquisition system to the periodic blood flow of the chicken heart is important. An ensemble of 50 images is obtained within 25 s, a time period where variations in conditions and physiological changes of the developing heart are negligible. An ensemble-correlation function is gained by summing up all cross-correlation functions of a specific interrogation window over a number of individual image-pairs. The ensemble-correlation

function is characterized by a much higher signal-to-noise ratio than the instantaneous cross-correlation functions, so that the measurement reliability can be greatly improved.

The effectiveness of the ensemble correlation method is evaluated by considering a measurement in the fully dilated ventricle. At this point of the cardiac phase the velocity is maximized and the tangential and radial velocity of the wall is minimized. The final velocity field is shown in the left part of Fig. 6, and will be discussed in detail in the Results section. The interrogation window was selected to be $64 \times 64$ pixels in size, with 50 percent overlap between subsequent interrogations, which leads to a 32 pixel vector spacing, equivalent to 20.6 μm (about one tenth of the inner lumen diameter). With a time difference of 0.5 ms between two frames, a velocity of 20 mm/s corresponds to a particle displacement of about 16 pixels, in correspondence to the optimal displacement recommended by Keane and Adrian (1992) for this interrogation window size. To get an estimate for the number of image pairs that are necessary to obtain a reliable velocity measurement, the percentage of valid data (where the correlated signal peak can be clearly identified with respect to the background noise) can be determined as a function of the number of image pairs that are considered for the ensemble correlation. In Fig. 4, the percentage of valid velocity vectors is plotted as a function of the number of summed correlation functions. Using a $64 \times 64$ pixel interrogation window size, only five image-pairs (corresponding to an acquisition time of 2.5 s) are sufficient to obtain more than 90% valid vectors under the current optical conditions. Using fifty image-pairs increases the validity ratio close to 100%, with little further improvement beyond this point. Smaller interrogation windows contain proportionally less information, therefore, obtaining a similar level of reliable vectors requires a

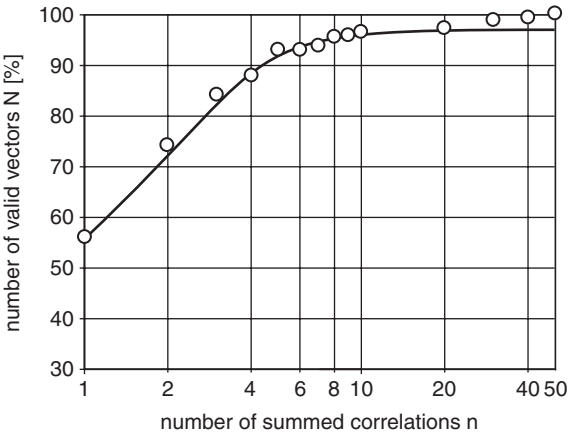


Fig. 4. Percentage of reliable vectors as a function of the number of summed correlation functions. If interrogation areas of $64 \times 64$ pixels are used, 50 image pairs are sufficient to obtain close to 100% reliabe vectors.

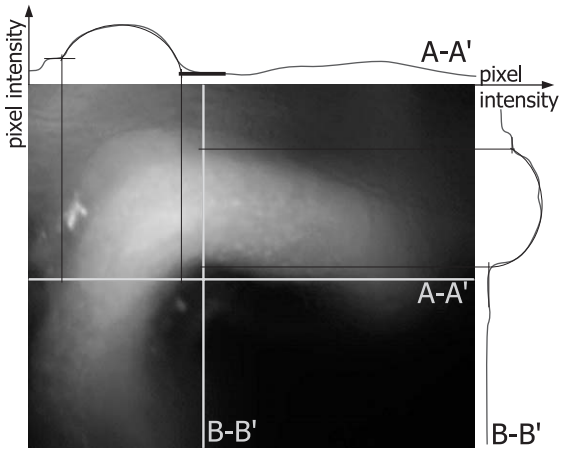


Fig. 5. The average of 100 image frames reveals the inner lumen boundary as a bright region. Due to the approximately circular cross-section of the vessel, the theoretical grey value intensity function has an elliptical shape. The intersection point of the theoretical intensity profile (least square fit to the data) and the grey level offset of the neighboring region accurately defines the position of the vessel wall.

corresponding increase in the number of images. Hence, the number of images that is required for the ensemble correlation further increases with decreasing size of the interrogation window (i.e., the curve in Fig. 4 shifts to the right).

The velocity data is also used for objectively determining the inner lumen boundary of the heart. Assuming the no-slip velocity condition at the wall, the wall position is readily available by extrapolating the measured velocity profile to zero. This approach was used by Stone et al. (2002) to determine wall positions with an accuracy approaching tens of nanometers. This method is only valid when the vessel walls are not moving (like in the fully expanded state), otherwise the image ensembles can be utilised for determining the wall position: By averaging over all image frames of the ensemble, the plasma region containing the fluorescent liposomes appears now as a bright region, while the rest of the image remains dark. The inner lumen boundary is then determined like shown in Fig. 5.

## 3. Results

Measurements are made at nine discrete points in the cardiac cycle, and are separated from each other by 50 ms. Each measurement represents the ensemble averaged evaluation of up to 50 image pairs with an interframing time of 0.5–4 ms, depending on the average magnitude of the velocities at a given point in the cycle. Given that a chicken embryo typically has a heart rate of 2 Hz, it follows that a single ensemble measurement requires 25 s to complete. The spatial resolution of the velocity data is estimated at $41 \times 41 \times 13\,\mu m^3$ (see the appendix).

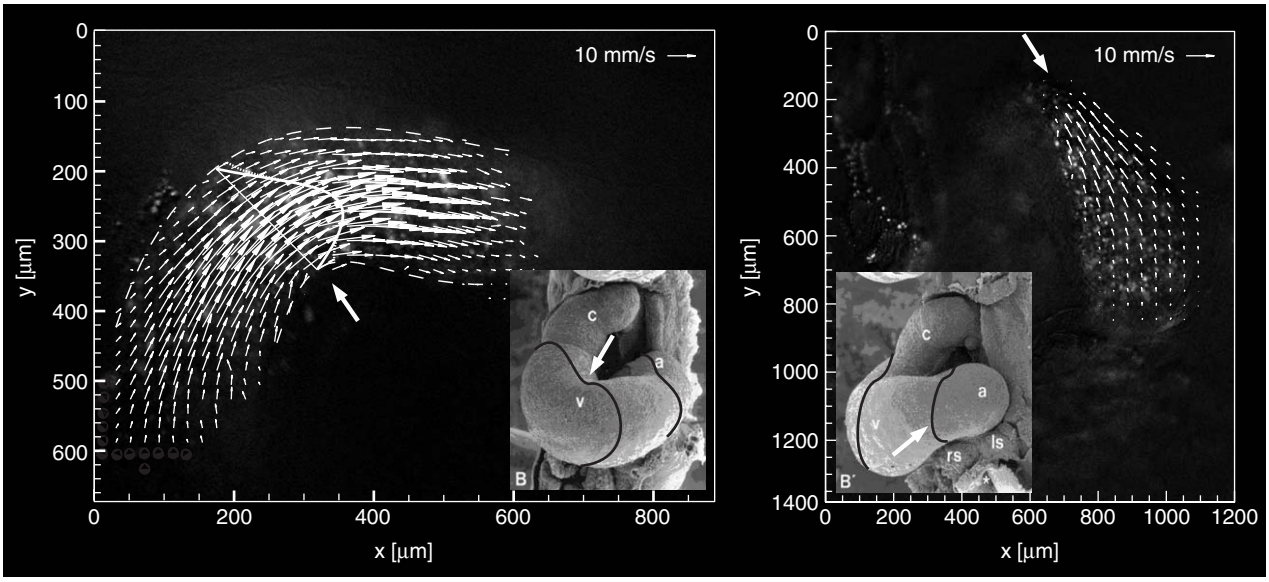


Fig. 6. Velocity distributions in the developing ventricle (left, 10× magnification) and in the atrium (right, 5× magnification) of a Stage 15 chicken embryo. A representative profile depicting the local ensemble-averaged, axis-normal velocity magnitude is superimposed on the vector field. The approximate lumen boundary is indicated by two dashed lines that are readily determined by interpolating the velocity profiles to zero. The location and spatial orientation of the measurement planes relative to the looping heart are indicated in the scanning electron micrographs from Männer (2000).

Fig. 7 gives an overview of the measured velocity distributions at different points in the embryonic cardiac cycle. The black lines mark the focused part of the inner surface of the endocardium. The flow enters from the left side of each image where the blood emerges perpendicular to the image plane. After crossing the measurement plane, the flow disappears again normal to the image plane in the direction of the pharyngeal arch arteries. The first frame of Fig. 7 shows the imaged part of the heart-tube being tightly closed. After 50 ms the tube is opened to a small slit, with the peak velocity rising to 3 mm/s.

It takes approximately 250 ms to fill the ventricle at these relatively low blood flow rates. When the imaged part of the tube is completely expanded (after 300 ms), a rapid peristaltic contraction has already started further upstream, providing a forward impetus that accelerates the fluid in the measurement plane to a peak velocity of 26 mm/s. The corresponding Reynolds number is about 0.5 at this point which indicates that this flow is mainly determined by viscous forces, but that inertia cannot be fully ignored. The Womersley number for the adjacent arteries is of order 0.2. The velocity map corresponding to this point of the cardiac cycle is shown in more detail in the left part of Fig. 6. The background shows a sample PIV image for orientation.

The dashed white lines in Fig. 6 mark the inner lumen boundary in the focused part of the endocardium. In our system only the velocity components parallel to the focal plane are measured. This explains why the axial velocity magnitude decreases to the left and to the right side of the flow field, as the main flow direction is not parallel to the focal plane in these regions. From the flow field, velocity profiles can be determined. At the cross-section indicated by a straight line, the flow is assumed to be parallel to the image plane, so that the third velocity component becomes zero. At this position a single velocity profile is superimposed as a continuous curve. The profile clearly shows an asymmetrical velocity distribution which suggests the highest shear stresses will appear at the inner curvature. Evidently, the conventional method of estimating the wall shear stress from the characteristic vessel diameter and the maximum velocity (as applies to fully developed laminar pipe flow) does not apply in this configuration.

The remaining portion of the cardiac cycle is depicted by the last two frames of Fig. 7. The peristaltic movement of the heart muscle enters the measurement plane from the left side and pushes the blood out to the right until the entire imaged portion of the tube is closed again.

Measurements in the developing atrium are found to be most successful in embryos that are lying on the side opposite the imaged atrium, with the head turned to the left, which naturally occurs in a small percentage of eggs. The right part of Fig. 6 shows an example of a velocity distribution in the expanding atrium. In contrast to the ventricle, the lumen boundary of the volume is more readily identified on the PIV-image of the atrium. This is explained by the smooth wall of the atrium, in contrast to the trabeculated myocardium of the ventricle. On the left side of the ventricle, just above

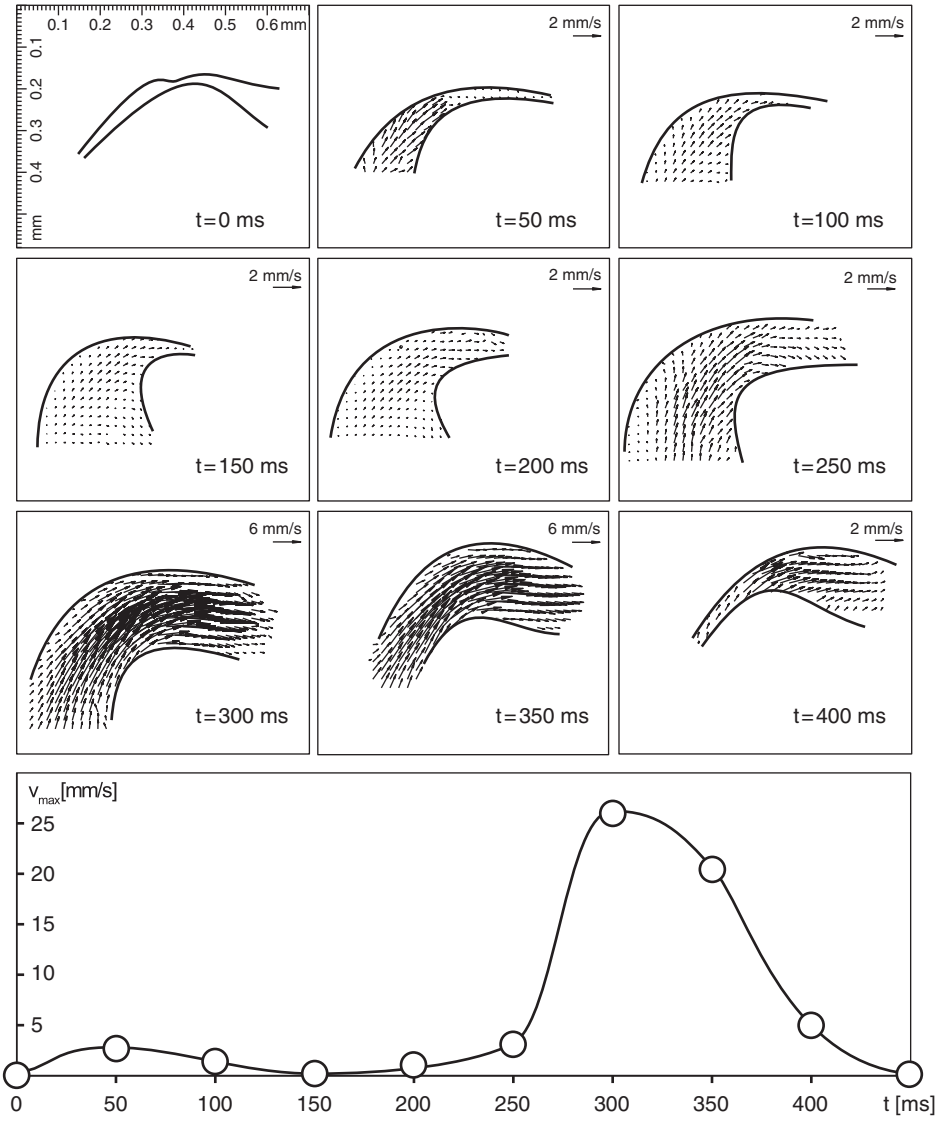


Fig. 7. Velocity distribution in the developing ventricle at nine succeeding points of the cardiac cycle. The vector plot at $t = 300$ ms complies the left part of Fig. 6. Note that the vector scale for $t = 300$ ms and $t = 350$ ms is reduced. The maximal velocity of each measurement is plotted over the time in the bottom part of the graph. The connecting curve serves to guide the eye.

the dashed line marking the inner ventricular wall, one can even see a group of particles trapped in the invaginations of the ventricle wall.

One of the goals of these measurements is to provide temporally and spatially resolved estimates of the velocity field. Under certain conditions these data can be used to access the local wall shear stress. To calculate these quantities, one needs to know the magnitude of the velocity gradient perpendicular to the wall and the local viscosity (see Eq. (1)). The velocity gradient can be estimated by quadratically extrapolating the flow profile to zero (Fig. 6 continuous velocity profile). The relatively large interrogation windows of $64 \times 64$ pixels lead to an overestimate of the near-wall velocity when the interrogation region partially extends out of the flow region (Fig. 6 dashed velocity profile). Under such circumstances, the estimated velocity equals the average velocity of the particle-containing region of the window. This effect is accounted for by omitting the affected vectors during the interpolation of the velocity profile. Alternatively, this effect can be corrected by relocating each biased velocity vector to the area within the interrogation window that most contributed to the correlation result (Lindken et al., 2003). For the case shown in Fig. 6, this results in a maximum strain rate of $1.0 \times 10^3\,\mathrm{s}^{-1}$ on the higher curvature wall. Here it should be pointed out that the strain rate can only be calculated for those regions where the main flow-direction is parallel to the image plane. The white, straight line in Fig. 6 indicates a section where the flow is

perfectly aligned with the flow. Assuming an effective dynamic blood viscosity of 5 mPa s leads to a maximum wall shear stress of 5 Pa. In comparison, the human vascular network experiences wall shear stress values up to approximately 7 Pa (Malek et al., 1999). The shear stress is estimated for the case of the totally dilated heart where we have found the highest velocities and therefore expect the largest magnitude of the wall shear stress during the cardiac cycle.

The assumption for the value of the dynamic blood viscosity represents a substantial contribution to the uncertainty of the shear stress estimate. Near the wall, a non-uniform distribution of erythrocytes accompanied by a spatial viscosity gradient must be expected, due to the Fåhraeus–Lindqvist effect. In the current estimate, a minimal value of the viscosity was assumed (corresponding to a magnitude slightly greater than that of clear plasma) in order to provide a conservative estimate of the wall shear stress. The non-Newtonian behavior of blood is less critical at shear rates that are relevant for the present study. Measurements from Chien (1970) show that at a shear rate above $1.0 \times 10^2\,s^{-1}$ neither aggregation occurs, nor can the deformability of the erythrocytes further decrease the viscosity. Therefore, taking in consideration the high shear rates we observed, the effective viscosity remains constant so that in this particular case the non-Newtonian behavior of blood can be ignored.

In the present measurements we encountered a broad size distribution of the tracer particles. In future work, improving the control of the tracer particle size will have several benefits: (1) Uniformly sized particles will allow for a higher number concentration for the same volume fraction of tracer particles and a much smaller interrogation window, increasing the spatial resolution; (2) The absence of large particles will also help minimize the effective depth of focus of the measurement plane to approximately 8 μm, as calculated from Eq. (A.1) (see the appendix) for the current optical set-up.

## 4. Discussion

In the post-genomics era, there exists not only an increasing interest in the functional aspects of (altered) gene expression, but also in the physical determinants of gene expression regulation. For example, lessons from knockout studies in mice have taught us the pivotal role of the growth hormone endothelin-1 in cardiovascular development (Yanagisawa et al., 1998), and in vitro studies with cultured endothelial cells showed a clear role for blood flow and shear stress on the regulation of endothelin-1 gene expression. This makes a role for shear stress in cardiovascular maldevelopment plausible, but evidence for that is still circumstantial. Here we present μPIV measurements that quantitatively resolve the instantaneous velocity distribution in a plane of the beating, embryonic avian heart. The novelty of these measurements is in the fact that the use of small fluorescent tracer particles and phase-locked cardiac synchronization demonstrates the potential to improve the effective temporal and spatial resolution over that of previously used methods for in vivo studies, and can extend such techniques to the more demanding highly unsteady flows within the early heart itself.

Groenendijk et al. (2004) found that high levels of mRNA for the Krüppel-like transcription factor (KLF-2) and endothelial Nitric Oxide Synthase (NOS3) were localized to the outflow tract and to other narrow parts of the heart and vasculature. These genes have been shown to upregulate expression under high shear stress conditions (Malek and Izumo, 1995; Dekker et al., 2002). In addition, these areas show low expression of endothelin-1, whose expression level has been shown to be negatively correlated with shear stress (Groenendijk et al., 2004). With the μPIV method described here, it will be possible to obtain definite data on the long-standing problem whether congenital cardiac and vascular anomalies are regulated independently or that they are mutually dependent through altered hemodynamics. Multi-plane μPIV measurements will enable the comprehensive investigation of the correlation of flow properties with gene expression patterns. The measurement method will definitely add to a better understanding of the role of hemodynamics in cardiogenesis in general.

With a single camera, two of three velocity components can be resolved. In case of vessel sections that are curved in only one plane or in the case of flat vessel networks, two-dimensional measurements are sufficient for comprehensively describing the flow. In other cases, where the flow is only perpendicular to the measurement plane at certain lines or points of the flow field, the orientation of the measurement plane might be adjusted parallel to the main flow direction in a certain region of interest. Such a general case is presented in this paper. The alignment of the measurement plane with the flow might be tedious or impossible in some cases. Nevertheless the two-dimensional projection of three velocity components might already contain most of the desired information.

The use of small fluorescent tracer particles has three principal advantages over the use of erythrocytes as tracer particles. The most important one comes with fluorescence; the small dimension of the liposomes leads to the other two advantages:

(1) Fluorescence allows the light emitted by the particles being separated from the light scattered by tissue and erythrocytes. In this way the signal-to-noise ratio of the particle images is increased, which

reduces ambiguity of the correlation result. The high signal-to-noise ratio also enables the usage of smaller particles.

(2) Small particles in a concentrated solution lead to a high information density in the PIV images. As a result, smaller interrogation windows can be used for the correlation which yields a higher resolution. In addition, it can be shown that the thickness of the measurement plane scales with the size of the tracer particles (see the appendix), which results in a much smaller effective measurement volume. Thus, the reduced particle size allows for both a higher information density and a thin, well-defined measurement plane, which improve the spatial resolution of the measurement.

(3) Small liposomes or particles of similar dimension (200–400 nm) penetrate the cell-depleted layer near the vessel wall and more closely follow the flow of plasma than much larger erythrocytes (8–10 μm). This is especially important for determining the wall shear stress from the near-wall velocity gradient.

## Acknowledgements

The authors would like to thank Patrick A.M. van Wieringen from *Leica* who generously provided the microscope, Ann L.B. Seynhaeve for preparing the lipsomal formulations, and Dr. Hans Vink for useful comments and suggestions during the preparation of the manuscript. This project is funded by the Dutch Technology Foundation STW (DSF.5695), the Netherlands Heart Foundation (NHF 2000.016; BPH, SS, BCWG), and the Dutch Cancer Foundation (DDHK2000-2224).

## Appendix. Resolution aspects

Every velocity vector that is obtained by means of PIV represents the average velocity of a particle pattern within a small evaluation volume with the side lengths $x$, $y$, and $z$. The dimension of the evaluation volume, which is equivalent to the resolution of the measurement, is determined by four factors: the magnification of the microscope objective, the pixel size of the camera, the width and length of the correlation window, and the thickness of the correlation plane.

The first three factors are determined by definite numbers and directly effect the length of $x$ and $y$. The thickness of the correlation plane, referred to as the depth of correlation, $\delta_{\mathrm{corr}}$, is in principle determined by the limited depth-of-focus of the microscope objective and can be calculated as suggested by Olsen and Adrian (2000) according to

$$\delta_{\mathrm{corr}} = 2\left[\frac{1-\sqrt{\varepsilon}}{\sqrt{\varepsilon}}\left(\left(\frac{1}{2NA}\right)^2 d_{\mathrm{p}}^2 + \frac{5.95(M+1)^2\lambda^2\left(\frac{1}{2NA}\right)^4}{M^2}\right)\right]^{1/2}. \quad \text{(A.1)}$$

The parameter $\varepsilon$ represents the ratio of the contribution to the correlation result of a particle in the focal plane and a particle at the edge of the measurement layer. Here, $d_{\mathrm{p}}$ is the particle diameter, $M$ the magnification, $NA$ the numerical aperture, and $\lambda$ is the wavelength of the light emitted by the particles. Although this relation is developed for a transparent fluid and uniform particle distribution and size, it is used to estimate the order of magnitude of $\delta_{\mathrm{corr}}$ for the present measurements.

By setting $\varepsilon$ to 0.1 (thus defining the influence of a particle on the correlation function to be insignificant if it drops below 10 per cent of the influence that a perfectly focused particle has), $\delta_{\mathrm{corr}}$, or the $z$ dimension of the measurement volume, is found to be 7 μm for a particle diameter of 400 nm, whereas erythrocytes of 8 μm diameter result in a 30 μm deep $z$-dimension. With a CCD-chip pixel size of 6.45 μm, a magnification of 10×, and an interrogation window size of 64 × 64 pixels, the $x$ and $y$ dimensions of the measurement volume are 41 μm. Doubling the magnification to 20× improves the $x$-, $y$-resolution to 21 μm. By increasing the particle density, the interrogation window size can be reduced to 32 × 32 pixels which also doubles the resolution, so that in combination with a 20× objective, a resolution of $10 \times 10 \times 7\,\mu\mathrm{m}^3$ $(x, y, z)$ is feasible.

Due to a broad size distribution of the currently utilised particles, a few larger tracers with a diameter of up to 3 μm gained influence on the correlation. The non-uniformity of the tracer particles does not significantly influence the accuracy of the measurements, but they lead to a thicker depth of correlation. Together with a 64 × 64 pixels interrogation window size, this leads to a resolution of $41 \times 41 \times 13\,\mu\mathrm{m}^3$ for the present experiments.

## References

Adrian, R.J., 1991. Particle-imaging techniques for experimental fluid mechanics. Annual Review of Fluid Mechanics 23, 261–304.

Chien, S., 1970. Shear dependence of effective cell volume as a determinant of blood viscosity. Science 168, 977–979.

Dekker, R., van Soest, S., Fontijn, R., Salamanca, S., de Groot, P., van Bavel, E., Pannekoek, H., Horrevoets, A., 2002. Prolonged fluid shear stress induces a distinct set of endothelial cell genes,

most specifically lung Krüppel-like factor (KLF2). Blood 100, 1689–1698.

Groenendijk, B., Hierck, B., Gittenberger-de Groot, A., Poelmann, R., 2004. Development-related changes in the expression of shear stress responsive genes KLF-2, ET-1, and NOS-3 in the developing cardiovascular system of chicken embryos. Developmental Dynamics 230 (1), 57–68.

Hamburger, V., Hamilton, H., 1951. A series of normal stages in the development of the chick embryo. Journal of Morphology 88, 49–92.

Hitt, D., Lowe, M., Tincher, J., Watters, J., 1996. A new method for blood velocimetry in the microcirculation. Microcirculation 3 (3), 259–263.

Hogers, B., DeRuiter, M., Gittenberger-de Groot, A., Poelmann, R., 1999. Extraembryonic venous obstructions lead to cardiovascular malformations and can be embryolethal. Cardiovascular Research 41, 87–99.

Hove, J., Köster, R., Forouhar, A., Acevedo-Bolton, G., Fraser, S., Gharib, M., 2003. Intracardiac fluid forces are an essential epigenetic factor for embryonic cardiogenesis. Nature 421, 172–177.

Keane, R., Adrian, R., 1992. Theory of cross-correlation analysis of PIV images. Applied Scientific Research 49, 191–215.

Liepsch, D. (Ed.), 1990. Blood Flow in Large Arteries: Application to Atherogenesis and Clinical Medicine. Monographs on Atherosclerosis. Karger, Basel.

Liepsch, D., 2002. An introduction to biofluid mechanics—basic models and applications. Journal of Biomechanics 35, 415–435.

Lindken, R., Poelma, C., Westerweel, J., 2003. Compensation for spatial effects for non-uniform seeding in PIV interrogation by signal relocation. In: Proceedings of the 5th International Symposium on Particle Image Velocimetry, September 2003, Busan, Korea.

Malek, A., Izumo, S., 1995. Control of endothelial cell gene expression by flow. Journal of Biomechanics 28, 1515–1528.

Malek, A., Alper, S., Izumo, S., 1999. Hemodynamic shear stress and its role in atherosclerosis. JAMA 282, 2035–2042.

Männer, J., 2000. Cardiac looping in the chick embryo: a morphological review with special reference to terminological and biomechanical aspects of the looping process. The Anatomical Record 259, 248–262.

Meinhart, C., Wereley, S., Santiago, J., 1999. PIV measurements of a microchannel flow. Experiments in Fluids 27, 414–419.

Meinhart, C., Wereley, S., Santiago, J., 2000. A PIV algorithm for estimating time-averaged velocity fields. Journal of Fluids Engineering 122, 285–289.

Olsen, M., Adrian, R., 2000. Out-of-focus effects on particle image visibility and correlation in microscopic particle image velocimetry. Experiments in Fluids 29 (Suppl. 7), 166–174.

Raffel, M., Willert, C., Kompenhans, J., 1998. Particle image velocimetry: a practical guide. Springer.

Santiago, J., Wereley, S., Meinhart, C., Beebe, D., Adrian, R., 1998. A particle image velocimetry system for microfluidics. Experiments in Fluids 25, 316–319.

Smith, M., Long, D., Damiano, E., Ley, K., 2003. Near-wall $\mu$-piv reveals a hydrodynamically relevant endothelial surface layer in venulus in vivo. Biophysical Journal 85, 637–645.

Stone, S., Meinhart, C., Wereley, S., 2002. A microfluidic-based nanoscope. Experiments in Fluids 33, 613–619.

Sugii, Y., Nishio, S., Okamoto, K., 2002a. Measurement of a velocity field in microvessels using a high resolution PIV technique. Annals of the New York Academy of Sciences 972, 331–336.

Sugii, Y., Nishio, S., Okamoto, K., 2002b. In vivo PIV measurements of red blood cell velocity field in microvessels considering mesentery motion. Physiological Measurement 23, 403–416.

Tangelder, G., Slaaf, D., Muijtjens, A., Arts, T., oude Egbrink, M., Reneman, R., 1986. Velocity profiles of blood platelets and red blood cells flowing in arterioles of the rabbit mesentery. Circulation Research 59 (5), 505–514.

Topper, J., Gimbrone Jr., M., 1999. Blood flow and vascular gene expression: fluid shear stress as a modulator of endothelial phenotype. Molecular Medicine Today 5 (1), 40–46.

Tretheway, D., Meinhart, C., 2002. Apparent fluid slip at hydrophobic microchannel walls. Physics of Fluids 14 (3), L9–L12.

Tsukada, K., Minamitani, H., Sekizuka, E., Oshio, C., 2000. Image correlation method for measuring blood flow velocity in microcirculation: correlation 'window' simulation and in vivo image analysis. Physiological Measurement 21, 459–471.

Ursem, N., Struijk, P., Poelmann, R., Gittenberger-de Groot, A., Wladimiroff, J., 2001. Dorsal aortic flow velocity in chick embryo of stage 16 to 28. Ultrasound in Medicine and Biology 27 (7), 919–924.

Westerweel, J., 1993. Digital Particle Image Velocimetry: Theory and Application. Delft University Press.

Westerweel, J., Geelhoed, P., Lindken, R., 2004. Single-pixel resolution ensemble correlation for micro-PIV applications. Experiments in Fluids 37 (3), 375–384.

Woodle, M., Lasic, D., 1992. Sterically stabilized liposomes. Biochimica et Biophysica Acta 1113 (2), 171–199.

Yanagisawa, H., Hammer, R., Richardson, J., Williams, S., Clouthier, D., Yanagisawa, M., 1998. Role of endothelin-1/endothelin-a receptor-mediated signaling pathway in the aortic arch patterning in mice. Journal of Clinical Investigation 102, 22–33.